Quantum Chemical Analysis of the Chemical Bonds in Tris(8-hydroxyquinolinato)aluminum as a Key Emitting Material for OLED

Jingping Zhang* and Gernot Frenking*

Faculty of Chemistry, Northeast Normal University, Changchun 130024, P. R. China, and Department of Chemistry, Philipps-University Marburg, Hans-Meerwein-Strasse, D-35042 Marburg, Germany

Received: March 7, 2004; In Final Form: May 6, 2004

The structures of *mer*-tris(8-hydroxyquinolinato)aluminum (Alq3) in the ground (S_0) and first excited (S_1) states have been optimized at the B3LYP/6-31+G(d) and CIS/6-31G(d) levels of theory. Absorption and emission for Alq3 are predicted with use of CI-ZINDO and TD-DFT. The results of an energy-partitioning analysis of the ground state of Alq3 are discussed. The electronic transition between S_0 and S_1 for *mer*-Alq3 is found to be mainly localized at the A-quinolate ligand as evidenced by the structural shift between the excited and ground states and the partial charge transfer from the phenoxide side to the pyridyl side within A-quinolate. The calculated optical and structural properties of *mer*-Alq3 are traced back to the weakest electrostatic attractive energy between the A-quinolate ligand and the Alq2 fragment due to the special arrangement, resulting in geometry change of ligand A upon excitation and the localization of the HOMO on A-quinolate.

1. Introduction

Organic light-emitting diode (OLED) is looked upon as a promising display technology, which is currently under intense investigation.[1] The emitting materials range from conjugated polymers[2,3] to small fluorescence molecules.[4] Tris(8-hydroxyquinolinato)aluminum (Alq3) is a milestone for the development of OLED, which was used as the electron-transport and emitting material in the first efficient low molecular weight OLED in 1987.[5] Since then, metaloquinolates have become a very important class of electroluminescent material in OLED,[6,7] with Alq3 being the most often used.[8]

After the rapid development of OLED in the past decade, studies of fundamental molecular properties of metaloquinolates have appeared in the literature in recent years.[9−23] The majority of the work carried out thus far has been on ground-state characteristics of Alq3. Alq3 has two geometric isomers, the facial (*fac*-Alq3) and meridianal (*mer*-Alq3) forms having C_3 and C_1 symmetry, respectively. The *mer*-Alq3 form was found to be the preferred form of Alq3, being energetically more stable than the facial structure. The *fac*-Alq3 can be reconverted for the most part to the meridianal molecule during evaporation onto unheated substrates or after dissolving it in polar solvents.[24] The vertical electronic excitation energies of Alq3 have been computed with molecular orbital methods.[16−20] In these theoretical studies, both the configuration interaction (CI) approach with the semiempirical method ZINDO[21] (CI-ZINDO) and the time-dependent density functional theory (TD-DFT) have been used to compute vertical excitation spectra[16−19] and the electroabsorption[20] of Alq3. Recently, the lowest singlet excited state (S_1) of Alq3 was optimized by using the singles configuration interaction (CIS) method.[22,23] Ab initio CIS, ZINDO, and TD-DFT methods were used to calculate emission energies and also the corresponding absorption energies.[22,23] The optimization of the S_0 and S_1 states of Alq3 at DFT and CIS have been carried out with 6-31G(d)[19] and 6-31G[23] basis sets, respectively.

Theoretical analyses of chemical bonding and reactivity have often been carried out at a qualitative level. By using modern methods of bonding analysis it is possible to obtain insights into the bonding situation of molecules which agree with the physical mechanisms of chemical bond formation. One such method is the energy partitioning scheme that is available in the program package ADF.[25,26] It is based on the work of Morokuma,[27] who suggested an energy partitioning procedure for Hartree−Fock wave functions. This work was later pursued by Ziegler and Rauk,[28] who showed that DFT calculations of interatomic interaction energies can be analyzed and interpreted in terms of physically meaningful contributions to the chemical bond. The energy partitioning analysis (EPA) has been proven to give an understanding of chemical bonds in terms of rigorously defined and physically meaningful contributions to the chemical bond in main-group and transition metal compounds.[29,30]

In this contribution, the energy partitioning analysis of the bonding between the metal fragment $Alq2^+$ and a single ligand q^- in Alq3 in its ground (S_0) state is performed. The meridianal isomer as shown in Figure 1 is considered, since only a racemic mixture of the *mer*-Alq3 has been confirmed by the crystal structure without solvent,[31] and the fact that *fac*-Alq3 can easily convert to the *mer* isomer.[24]

2. Computational Details

The geometry of *mer*-Alq3 in the S_0 ground state was optimized by using the hybrid B3LYP functional[32,33] with 6-31G+(d) basis sets.[34] For the geometry optimization of the first singlet excited state (S_1), configuration interaction with all singly excited determinants[35] (CIS) was used with 6-31G(d) basis sets.[36,37] To obtain estimates of the vertical electronic excitation energies of *mer*-Alq3, time-dependent density functional theory (TD-DFT)[38] using B3LYP was used with both

* Address correspondence to these authors at the following e-mail addresses: zhangjp162@nenu.edu.cn and frenking@chemie.uni-marburg.de.

10.1021/jp0489774 CCC: $27.50
Published on Web 10/20/2004

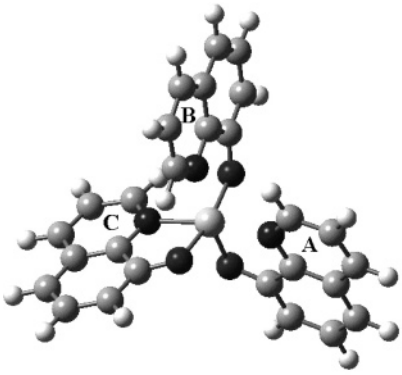

Figure 1. The geometry of *mer*-Alq3 with labels A−C for three quinolate ligands

6-31G(d) and 6-31+G(d) basis sets. To compare with previous results for Alq3, calculations of the vertical electronic excitation energies of the S_0 and S_1 states were also carried out by using configuration interaction including single excitations with an active space of (a) 15 occupied and 15 unoccupied molecular orbitals and (b) all valence and all unoccupied orbitals in the active space with the semiempirical method ZINDO, respectively. The above calculations were carried out with Gaussian 98.[39]

To perform an energy decomposition analysis of the chemical bonds, the calculation for the optimized ground state has been carried out at the BP86[40,41] level of DFT, using a valence basis set of TZ2P quality with the frozen-core approximation.

The bonding interactions between the metal fragment $Alq2^+$ and a single ligand q^- have been analyzed with the energy decomposition scheme of the program package ADF[25,26] which is based on the EDA method of Morokuma[27] and the ETS partitioning scheme of Ziegler.[28] The bond dissociation energy ΔE between two fragments A and B is partitioned into several contributions which can be identified as physically meaningful entities. First, ΔE is separated into two major components ΔE_{prep} and ΔE_{int}:

$$\Delta E = \Delta E_{prep} + \Delta E_{int} \quad (1)$$

ΔE_{prep} is the energy that is necessary to promote the fragments A and B from their equilibrium geometry and electronic ground state which they have in the compound AB. ΔE_{int} is the instantaneous interaction energy between the two fragments in the molecule. The latter quantity is the focus of the bonding analysis. The interaction energy ΔE_{int} can be divided into three main components:

$$\Delta E_{int} = \Delta E_{elstat} + \Delta E_{pauli} + \Delta E_{orb} \quad (2)$$

ΔE_{elstat} gives the electrostatic interaction energy between the fragments calculated with a frozen electron density distribution in the complex. ΔE_{pauli} gives the repulsive interactions between the fragments which are caused by the fact that two electrons with the same spin cannot occupy the same region in space. The term comprises the four-electron destabilizing interactions between occupied orbitals. ΔE_{pauli} is calculated by enforcing the Kohn−Sham determinant of AB, which results from superimposing fragments A and B to be orthonormal through antisymmetrization and renormalization. The stabilizing orbital interaction term ΔE_{orb} is calculated in the final step of the EPA analysis when the Kohn−Sham orbitals relax to their form. Further details of the method can be found in the literature.[26]

TABLE 1: Selected Optimized Bond Lengths (Å) and Bond Angles (deg) for *mer*-Alq3 at B3LYP/6-31+G(d) (Alq3-L) and Experimental Data from X-ray Structure Analysis (Alq3-λ_{exp}) [31]

	Alq3-A	Alq3-B	Alq3-C	Alq3-A_{exp}	Alq3-B_{exp}	Alq3-C_{exp}
O−Al	1.859	1.882	1.886	1.850	1.860	1.857
N−Al	2.083	2.126	2.065	2.050	2.087	2.017
Oa−Al−Nb	172.62			171.46		
Ob−Al−Oc	166.60			168.22		
Na−Al−Nc	170.63			173.82		
Oa−Al−Na	83.12			83.63		
Ob−Al−Nb	80.41			81.36		
Oc−Al−Nc	82.47			83.43		

3. Results and Discussion

3.1. Geometries of *mer*-Alq3 in the S_0 and S_1 States. The molecule *mer*-Alq3 is a trischelate organic complex that possesses C_1 symmetry in which the central trivalent aluminum atom has a distorted octahedral coordination. The structure of *mer*-Alq3 is shown in Figure 1, where labels A−C are used to denote the three different quinolate ligands. The nitrogen atoms of A- and C-quinolate and oxygen atoms of B- and C-quinolate are trans to each other. Selected optimized bond lengths and bond angles at B3LYP/6-31+G(d) for the S_0 ground state of *mer*-Alq3 are given in Table 1, along with the Al−O and Al−N distances which have been determined from X-ray structure analysis.[31] The agreement between the calculated and experimental data is quite good. The theoretical bond lengths are a bit longer than the experimental values, which is at least partly due to solid-state effects.[42] The ground-state structure of *mer*-Alq3 has been studied in previous theoretical work[9,12,14,19,22] where only the bond lengths but no bond angles were given.

Table 2 summarizes the optimized bond lengths of the ground state of *mer*-Alq3 at the HF/6-31G(d) level and the bond lengths of the excited state at the CIS/6-31G(d) level. The positive and negative values in the ΔL_{E-G} (L = A, B, C) columns indicate bond elongation and contraction in the excited state for A-, B-, and C-quinolates in *mer*-Alq3, respectively. Figure 2 gives the scheme of the quinolato ligand and the atom labels used in Table 2. The comparison of the S_0 and S_1 state geometries for A-, B-, and C-quinolates in *mer*-Alq3 indicates that the structural shift is predominantly localized at the A-quinolate. The B- and C-quinolates in *mer*-Alq3 are only slightly affected except for changes in the Al−O and Al−N bond lengths. The changes of the bond lengths between the S_0 and S_1 state are in agreement with previous investigation.[22] The change of bond angles between S_0 and S_1 is found predominantly in the A-quinolate, with the largest difference of 3.7°. Thus, the excitation from the S_0 to the S_1 state yields significant structural changes in only one ligand while the other two ligands remain nearly the same. We want to point out that the predominant relaxation of ligand A in the S_1 state compared with that in S_0 may contribute to the observed large Stokes shift (126 nm) between the optical emission spectra and absorption spectra.

Table 3 shows the calculated atomic partial charges in the S_0 and S_1 states. Larger differences of the charges are mainly found in A-quinolate, while those of the B- and C-ligands are negligibly small. The larger positive (C_5, O) and negative (N_1, C_2, C_4) values of ΔA_{E-G} correspond to the partial charge transfer from the phenoxide side to the pyridyl side within A-quinolate. This clearly indicates that the structural distortion in *mer*-Alq3 is caused by the exciton localization in the A-ligand rather than by charge separation between Al and three ligands. The reason for this will be explained in detail in section 3.3.

3.2. Frontier Molecular Orbital (FMO) Analyses and Optical Properties of the S_0 and S_1 States. The excited state

TABLE 2: Optimized Bond Lengths (Å) of *mer*-Alq3 in the S_0 Ground State (L_G) and S_1 Excited Electronic States (L_E) at HF/6-31G(d) and CIS/6-31G(d), Respectively, and Differences between the S_0 and S_1 States (ΔL_{E-G})

	A_G	A_E	ΔA_{E-G}	B_G	B_E	ΔB_{E-G}	C_G	C_E	ΔC_{E-G}
N_1-C_2	1.298	1.376	0.078	1.300	1.300	0.000	1.298	1.298	0.000
C_2-C_3	1.409	1.358	−0.051	1.411	1.410	−0.001	1.411	1.411	0.000
C_3-C_4	1.361	1.419	0.058	1.363	1.363	0.000	1.362	1.362	0.000
C_4-C_{10}	1.416	1.400	−0.016	1.417	1.417	0.000	1.417	1.417	0.000
$C_{10}-C_5$	1.417	1.405	−0.012	1.418	1.418	0.000	1.418	1.418	0.000
C_5-C_6	1.363	1.422	0.059	1.364	1.364	0.000	1.363	1.363	0.000
C_6-C_7	1.412	1.358	−0.054	1.414	1.414	0.000	1.415	1.415	0.000
C_7-C_8	1.372	1.442	0.070	1.372	1.372	0.000	1.371	1.371	0.000
C_8-C_9	1.431	1.428	−0.003	1.428	1.429	0.001	1.430	1.429	−0.001
C_9-C_{10}	1.399	1.417	0.018	1.397	1.397	0.000	1.395	1.396	0.001
N_1-C_9	1.357	1.338	−0.019	1.352	1.353	0.001	1.353	1.352	−0.001
C_8-O	1.299	1.262	−0.037	1.301	1.301	0.000	1.304	1.304	0.000
O−Al	1.826	1.904	0.078	1.849	1.855	0.006	1.855	1.852	−0.003
N_1-Al	2.106	2.012	−0.094	2.166	2.117	−0.049	2.076	2.109	0.033

TABLE 3: NBO Charges of the Ligands for *mer*-Alq3 in the Ground (S_0) and First Excited (S_1) States and Charge Differences between the S_0 and S_1 States (ΔL_{E-G}), Calculated at HF/6-31G and CIS/6-31G, Respectively, and Total NBO Charges on Al and Each Ligand (q_{LX})

	A_G	A_E	ΔA_{E-G}	B_G	B_E	ΔB_{E-G}	C_G	C_E	ΔC_{G-E}
N_1	−0.599	−0.765	−0.166	−0.607	−0.618	−0.011	−0.615	−0.609	0.006
C_2	0.111	0.014	−0.097	0.106	0.115	0.009	0.126	0.123	−0.003
C_3	−0.314	−0.287	0.027	−0.315	−0.316	−0.001	−0.312	−0.314	−0.002
C_4	−0.130	−0.304	−0.174	−0.133	−0.129	0.004	−0.131	−0.132	−0.001
C_5	−0.299	−0.105	0.194	−0.295	−0.292	0.003	−0.290	−0.290	0.000
C_6	−0.181	−0.257	−0.076	−0.184	−0.186	−0.002	−0.187	−0.189	−0.002
C_7	−0.335	−0.238	0.097	−0.337	−0.336	0.001	−0.338	−0.337	0.001
C_8	0.440	0.511	0.071	0.425	0.424	−0.001	0.424	0.422	−0.002
C_9	0.140	0.175	0.035	0.128	0.135	0.007	0.140	0.139	−0.001
C_{10}	−0.077	−0.111	−0.034	−0.081	−0.082	−0.001	−0.080	−0.082	−0.002
O	−0.942	−0.807	0.135	−0.944	−0.945	−0.001	−0.955	−0.951	0.004
H_2	0.236	0.227	−0.009	0.263	0.263	0.000	0.260	0.261	0.001
H_3	0.253	0.243	−0.010	0.256	0.256	0.000	0.255	0.255	0.000
H_4	0.249	0.235	−0.014	0.251	0.251	0.000	0.249	0.249	0.000
H_5	0.237	0.244	0.007	0.240	0.240	0.000	0.239	0.239	0.000
H_6	0.241	0.251	0.010	0.243	0.243	0.000	0.242	0.242	0.000
H_7	0.253	0.261	0.008	0.255	0.253	−0.002	0.251	0.252	0.001
Al	S_0 2.168				S_1 2.160				
q_{LX}	q_{AG} −0.717	q_{BG} −0.713	q_{CG} −0.729		q_{AE} −0.724		q_{BE} −0.724		q_{CE} −0.722

properties of Alq3 have been intensively investigated by photoabsorption, photoluminescence, and electroluminescence techniques.[6,14,16,19,31,43−49] The experimental absorption spectrum of vacuum deposited Alq3 thin films showed a maxima at 385 nm.[48] Solution-phase investigations revealed an absorption maximum at 390 nm, in close agreement with the results of thin film measurement.[44] The experimental photoluminescence emission in solution was observed at 514 nm[44] and the electroluminescence emission in devices was recorded at 519 nm.[6] We calculated the absorption and emission wavelengths and the frontier molecular orbitals (FMOs) for *mer*-Alq3 using the optimized geometries of the S_0 and S_1 states, respectively. A graphical display of the FMOs of the S_0 and S_1 states is shown in Figures 3 and 4. The calculated absorption and emission wavelengths using CI-ZINDO and TD-DFT are summarized in Table 4.

The FMO distribution of the S_0 state shown in Figure 3 suggests a localization of molecular orbitals at each quinolate ligand. The HOMO is localized mainly at the A-ligand, whereas HOMO-1 and HOMO-2 are predominantly at the C- and B-ligand, respectively. Moreover, the LUMO is localized mainly at the B-ligand while LUMO+1 and LUMO+2 are localized mainly at the C- and A-ligand, respectively. This pattern is in

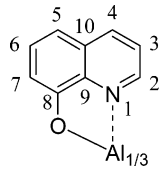

Figure 2. Structure and labels for each ligand (L refers to A, B, or C) in *mer*-Alq3

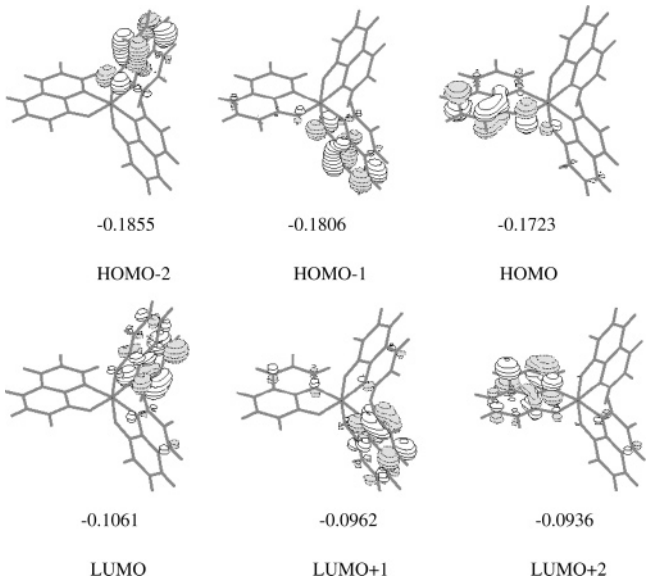

Figure 3. Frontier molecular orbitals (FMOs) and their energies (hartree) for the ground state (S_0) of *mer*-Alq3 obtained by BP86/T2ZP with a small core (isocontour value 0.05).

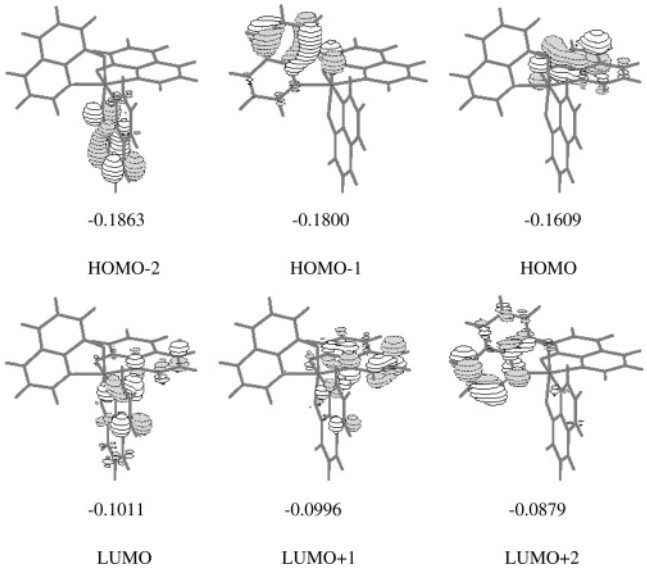

Figure 4. Frontier molecular orbitals (FMOs) and their energies (hartree) for the first excited state (S_1) of *mer*-Alq3 obtained by BP86/T2ZP with a small core (isocontour value 0.05).

TABLE 4: Comparison of the Calculated Absorption and Emission Wavelengths of *mer*-Alq3 in S_0 (λ_a) and S_1 (λ_e) from the Current Investigation with Previous Calculations with CI-ZINDO and TD-DFT and Experimental Results

methods	λ_a (nm)	λ_e (nm)
CI-ZINDO	407 (385),[a] 356,[b] 377,[c] 386[d]	498 (461),[a] 484[d]
TD-B3LYP/6-31G(d)	429, 427[e]	533
TD-B3LYP/6-31+G(d)	436	543
TD-B3LYP/3-21+G**	415[f]	538[f]
experiments	390,[g] 385[h]	514,[g] 519[i]

[a] The ZINDO calculation results with the 15 occupied and 15 unoccupied molecular orbitals are given in parentheses for current study. [b] Reference 20. [c] Reference 16. [d] Reference 23. [e] Reference 19. [f] Reference 22. [g] Reference 44. [h] Reference 47. [i] Reference 6

agreement with a previous DFT study published by Curioni et al.[9] The spatial overlap between HOMO and LUMO is weak. As a result, the stronger optical absorption does not correspond to the transition from HOMO to LUMO, but from HOMO to LUMO+2 on the A-ligand.

The shape of the FMO for the S_1 state shown in Figure 4 demonstrates that the energy sequence of each ligand and the extent of localization for the MO are different from those in the S_0 state due to the relaxation of the structure on ligand A. The HOMO of the S_1 state is localized mainly on the phenoxide side of the A-ligand while the HOMO-1 and HOMO-2 are predominantly on the phenoxide sides of the B- and C-ligand, respectively. The LUMO is distributed over both pyridyl sides of the A- and C-ligands. The LUMO+1 is localized mainly at the pyridyl sides of the A-ligand and to some extent at the C-ligand. The LUMO+2 is localized predominantly at the pyridyl side of the C-ligand. This type of electron distribution favors the optical transition between HOMO and LUMO.

The vertical electronic excitation energy for *mer*-Alq3 calculated with CI-ZINDO including all single configurations from the highest 15 occupied and lowest 15 virtual orbitals (15/15) is 385 nm. The CI-ZINDO value including all valence and all unoccupied orbitals in the active space is 407 nm. The calculated values of 385 and 407 nm for the lowest lying vertical electronic excitations are in good agreement with the experimental results of 385−390 nm. The emission energy calculated with CI-ZINDO (15/15) is 461 nm, which deviates somewhat from the experimental values 514 and 519 nm.[6,44] A better agreement with experiment is found when all valence and all unoccupied orbitals are included in the active space, which yields a theoretical result of 498 nm (Table 4). The difference between the calculated absorption and emission wavelengths at CI-ZINDO (76 and 91 nm) can be compared with the experimental Stokes shift for Alq3 in solution, which is 126 nm.[44] These calculations suggest that CI-ZINDO considering all valence and unoccupied orbitals in the active space gives a reasonable excitation energy for the transition between the S_0 and S_1 states. It is worth noting that the excited state is optimized under gas phase, and as a result, the structural shift may be to some extent favored over than that in the solution or solid phase. Therefore, the calculated emission energy by CI-ZINDO deviates somewhat from the experimental values.

TABLE 5: Energy Partitioning Analysis of *mer*-Alq3 in the Electronic Ground State at BP86/*T*2ZP, Using the Fragments q_{L1}^- and $Alq_{L2}q_{L3}^+$ (all values in kcal/mol unless otherwise indicated)

	q_a^--$Alq_bq_c^+$	q_b^--$Alq_aq_c^+$	q_c^--$Alq_aq_b^+$
ΔE_{int}	−192.4	−190.8	−194.4
ΔE_{Pauli}	152.5	157.1	158.0
ΔE_{elstat}	−215.3	−219.1	−221.5
ΔE_{orb}	−129.6	−128.8	−130.9
ΔE_{elstat}, %	62.4	63.0	62.9
ΔE_{orb}, %	37.6	37.0	37.1

The analyses of the lowest lying $\pi-\pi^*$ electronic transitions presented here based on the CI-ZINDO calculations are as follows: HOMO → LUMO+2 (62%), HOMO-2 → LUMO (27%), and HOMO → LUMO+1 (10%). Thus, the $\pi-\pi^*$ transition occurs mainly at the A-quinolate ligand, which is in good agreement with the shape of the FMOs (see Figure 3). However, the assignment of the electronic transitions for *mer*-Alq3 by using the geometry of the excited state optimized at CIS/6-31G(d) is the $\pi-\pi^*$ transition between HOMO and LUMO (see Figure 4). This comes from the different electron distribution upon the geometrical relaxation or change of the excited state on ligand A. The optical properties of *mer*-Alq3 are in good agreement with the change of the NBO charge distribution.

Table 4 gives also the calculated absorption and emission wavelengths of *mer*-Alq3, using TD-B3LYP with 6-31G(d) and 6-31+G(d) basis sets. The absorption wavelength is predicted at 429 and 436 nm, respectively. The assignments of the lowest $\pi-\pi^*$ electronic transitions are as follow: HOMO-2 → LUMO, HOMO-1 → LUMO, HOMO → LUMO+1, and HOMO → LUMO+2. The emission energy is predicted to be ca. 533 and 543 nm by 6-31G(d) and 6-31+G(d) basis set, respectively. The assignment of possible $\pi-\pi^*$ electronic transitions by using the excited-state structure optimized at CIS/6-31G(d) is HOMO → LUMO and HOMO → LUMO+1 (see Figure 4). The estimated Stokes shifts at the TD-B3LYP level of theory are ca. 104 and 107 nm, which is in good agreement with the experimental value.

3.3. Energy Partitioning Analysis of *mer*-Alq3. To explore the nature of the metal−ligand interaction in *mer*-Alq3, we carried out an energy partitioning analysis of the interaction energy. Table 5 gives the most important results of the bonding analysis for the interactions between one quinolate ligand (q_{L1}^-) and the $Alq_{L2}q_{L3}^+$ (q_{Li} = A or B or C) fragment.

The results show that the electrostatic energy plays a more important role for the metal−ligand binding than for the orbital interaction, i.e., the metal−ligand interactions have a larger electrostatic character than covalent character. Note that the electrostatic interaction energy (ΔE_{elstat}) between q_a and Alq_bq_c fragments is weaker than those of q_b-Alq_aq_c and q_c-Alq_aq_b. It is

suggested that the overall arrangement for three ligands is responsible to the weaker ΔE_{elstat} between q_a and Alq_bq_c fragments. The weaker attractive energy between q_a and Alq_bq_c fragments results in the HOMOs localizing on the A-ring for both S_0 and S_1 states, thus the geometry change may easily occur upon excitation of *mer*-Alq3 for ligand A. This result also can be used to explain the previous calculation, where the doped metal atom prefers to interact with the A-quinolate ligand.[12] It is worth noting that the weaker electrostatic interaction between the A-quinolate ligand and the Mq2 has been further confirmed by other 13-group metals, and will be addressed in a separate publication elsewhere.

4. Summary and Conclusion

The ground and first singlet excited state of *mer*-Alq3 have been optimized by using the B3LYP/6-31+G(d) and CIS/6-31G(d) levels of theory. The electronic excitation for the ground state and the emission of the excited state for *mer*-Alq3 have been simulated by CI-ZINDO and TD-B3LYP approaches and interpreted in terms of the nature of the FMOs and bond analyses. For CI-ZINDO and the TD-B3-LYP level of theories, the calculated wavelength for absorption and emission wavelengths agree very well with experiment. Therefore, further quantum chemical calculations based on this step would be useful for the design of emissive compounds, such as tuning the emission energies of Alq3 derivatives. The $S_0 \rightarrow S_1$ excitation is found to be mainly localized on the A-quinolate ligand as evidenced by the structural shift and the NBO charge difference between the excited and ground electronic states of *mer*-Alq3. The energy partitioning analysis suggests that the metal−ligand interactions of *mer*-Alq3 have a higher electrostatic character than covalent character. The nature of the A-quinolate ligand, which plays an important role in the optical properties of *mer*-Alq3, perhaps can be explained by the weaker electrostatic attraction between the A-quinolate ligand and the Alq2 fragment due to the overall arrangement, resulting in the geometry change upon excitation on ligand A.

Acknowledgment. Financial support from the National Natural Science Foundation of China (No. 50473032), the SRF for ROCS and SEM, an Outstanding Youth Project of Jinlin Province, are gratefully acknowledged. J. Zhang thanks the DAAD for financial support and V. M. Rico, C. Esterhuysen, and M. Lein for kind help in using the program ADF.

References and Notes

(1) Miyata, S.; Nalwa, S. *Organic Electroluminescent Materials and Devices*; Gordon and Breach: Amsterdam, The Netherlands, 1997.

(2) Burroughes, J. H.; Bradley, D. D. C.; Brown, A. R.; Marks, R. N.; Mackay, K.; Friend, R. H.; Burns, P. L.; Holmes, A. B. *Nature* **1990**, *347*, 539.

(3) Friend, R. H.; Gymer, R. W.; Holmes, A. B.; Burroughes, J. H.; Marks, R. N.; Taliani, C.; Bradley, D. D. C.; Dos Santos, D. A.; Bredas, J. L.; Logdlund, M.; Salaneck, W. R. *Nature* **1999**, *397*, 121.

(4) Mitsche, U.; Baeuerle, P. *J. Mater. Chem.* **2000**, *10*, 1471.

(5) Tang, C. W.; Van Slyke, S. A. *Appl. Phys. Lett.* **1987**, *51*, 913.

(6) Hamada, Y. *IEEE Trans. Electron Devices*, **1997**, *44*, 1208.

(7) Chen, C. H.; Shi, J. *Coord. Chem. Rev.* **1998**, *171*, 161.

(8) Van Slyke, S. A.; Chen, C. H.; Tang, C. W. *Appl. Phys. Lett.* **1996**, *69*, 2160.

(9) Curioni, A.; Boero, M.; Andreoni, W. *Chem. Phys. Lett.* **1998**, *294*, 263.

(10) Curioni, A.; Andreoni, W. *J. Am. Chem. Soc.* **1999**, *121*, 8216.

(11) Curioni, A.; Andreoni, W.; Treusch, R.; Himpsel, R. F.; Haskal, E.; Seidler, P.; Kakar, S.; van Buuren, T.; Terminello, L. J. *Appl. Phys. Lett.* **1998**, *72*, 1575.

(12) Johansson, N.; Osada, T.; Stafstrom, S.; Salaneck, W. R.; Parente, V.; dos Santos, D. A.; Crispin, X.; Bredas, J. L. *J. Chem. Phys.* **1999**, *111*, 2157.

(13) Halls, M. D.; Aroca, R. *Can. J. Chem.* **1998**, *76*, 1730.

(14) Kushto, G. P.; Iizumi, Y.; Kido, J.; Kafafi, Z. H. *J. Phys. Chem. A* **2000**, *104*, 3670.

(15) Amati, M.; Lelj, F. *Chem. Phys. Lett.* **2002**, *363*, 451.

(16) Burrows, P. E.; Shen, Z.; McCarty, D. M.; Forrest, S. R.; Cronin, J. A.; Thompson, M. E. *J. Appl. Phys.* **1996**, *79*, 7991.

(17) Su, Z.; Cheng, H.; Gao, H.; Sun, S.; Chu, B.; Wang, R.; Wang, Y. *Gaodeng Xuexiao Huaxue Xuebao*, **2000**, *211*, 416.

(18) Anderson, S.; Weaver, M. S.; Hudson, A. J. *Synth. Met.* **2000**, *111*−*112*, 459.

(19) Martin, R. L.; Kress, J. D.; Campbell, I. H.; Smith, D. L. *Phys. Rev. B* **2000**, *61*, 15804.

(20) Stampor, W.; Kalinowski, J.; Marconi, G.; Di Marco, P.; Fattori, V.; Giro, G. *Chem. Phys. Lett.* **1998**, *283*, 373.

(21) Bacon, A. D.; Zerner, M. C. *Theor. Chim. Acta* **1979**, *53*, 21.

(22) Halls, M. D.; Schlegel, H. B. *Chem. Mater.* **2001**, *13*, 2632.

(23) Sugimoto, M.; Sakaki, S.; Sakanoue, K.; Newton, M. D. *J. Appl. Phys.* **2001**, *90*, 6092.

(24) Cölle, M.; Dinnebier, R. E.; Brütting, W. *Chem. Commun.* **2002**, 2908.

(25) Bickelhaupt, F. M.; Baerend, E. J. *Rev. Comput. Chem.* **2000**, *15*, 1.

(26) te Velde, G.; Bickelhaupt, F. M.; Baerend, E. J.; van Gisbergen, S. J. A.; Guerra, C. F.; Snijder, J. G.; Ziegler, T. *J. Comput. Chem.* **2001**, *22*, 931.

(27) Morokuma, K. *J. Chem. Phys.* **1971**, *55*, 1236.

(28) Ziegler, T.; Rauk, A. *Theor. Chim. Acta* **1977**, *46*, 1.

(29) (a) Diefenbach, A.; Bickelhaupt, F. M.; Frenking, G. *J. Am. Chem. Soc.* **2000**, *122*, 6449. (b) Chen, Y.; Frenking, G. *J. Chem. Soc., Dalton Trans.* **2001**, 434. (c) Lein, M.; Frunzke, J.; Timoshkin, A.; Frenking, G. *Chem. Eur. J.* **2001**, *7*, 4155. (d) Uddin, J.; Frenking, G. *J. Am. Chem. Soc.* **2001**, *123*, 1683. (e) Doerr, M.; Frenking, G. *Z. Allg. Anorg. Chem.* **2002**, *628*, 843. (f) Frenking, G.; Wichmann, K.; Fröhlich, N.; Grobe, J.; Golla, W.; Le Van, D.; Krebs, B.; Laege, M. *Organometallics* **2002**, *21*, 2921. (g) Frunzke, J.; Lein, M.; Frenking, G. *Organometallics* **2002**, *21*, 3351. (h) Loschen, C.; Voigt, K.; Frunzke, J.; Diefenbach, A.; Diedenhofen, M.; Frenking, G. *Z. Allg. Anorg. Chem.* **2002**, *628*, 1294. (i) Rayon, V. M.; Frenking, G. *Chem. Eur. J.* **2002**, *8*, 4693. (j) Cases, M.; Frenking, G.; Duran, M.; Sola, M. *Organometallics* **2002**, *21*, 4182. (k) Bessac, F.; Frenking, G. *Inorg. Chem.* **2003**, *42*, 7990. (l) Frenking, G.; Wichmann, K.; Froehlich, N.; Loschen, C.; Lein, M.; Frunzke, J.; Rayon, V. M. *Coord. Chem. Rev.* **2003**, *238*−*239*, 55.

(30) (a) Bickelhaupt, F. M.; Radius, U.; Ehlers, A. W.; Hoffmann, R.; Baerends, E. J. *New J. Chem.* **1998**, *22*, 1. (b) Radius, U.; Bickelhaupt, F. M.; Ehlers, A. W.; Goldberg, N.; Hoffmann, R. *Inorg. Chem.* **1998**, *37*, 1080. (c) Ehlers, A. W.; Baerends, E. J.; Bickelhaupt, F. M.; Radius, U. *Chem. Eur. J.* **1998**, *4*, 210. (d) Dickinson, A. A.; Willock, D. J.; Calder, R. J.; Aldridge, S. *Organometallics* **2002**, *21*, 1146.

(31) Brinkmann, M.; Gadret, G.; Muccini, M.; Taliani, C.; Masciocchi, N.; Sironi, A. *J. Am. Chem. Soc.* **2000,** *122*, 5147.

(32) Becke, A. D. *J. Chem. Phys.* **1993**, *98*, 5648.

(33) Lee, C.; Yang, W.; Parr, R. G. *Phys. Rev. B* **1988**, *37*, 785.

(34) Petersson, G. A.; Bennett, A.; Tensfeldt, T. G.; Al-Laham, M. A.; Shirley, W. A.; Mantzaris, J. *J. Chem. Phys.* **1988**, *89*, 2193.

(35) Foresman, J. B.; Head-Gordon, M.; Pople, J. A.; Frisch, M. J. *J. Phys. Chem.* **1992**, *96*, 135.

(36) Hehre, W. J.; Ditchfield, R.; Pople, J. A. *J. Chem. Phys.* **1972**, *56*, 2257.

(37) Francl, M. M.; Petro, W. J.; Hehre, W. J.; Binkley, J. S.; Gordon, M. S.; DeFrees, D. J.; Pople, J. A. *J. Chem. Phys.* **1982**, *77*, 3654.

(38) Stratmann, R. E.; Scuseria, G. E.; Frisch, M. J. *J. Chem. Phys.* **1998**, *109*, 8218.

(39) Frisch, M. J.; Trucks, G. W.; Schlegel, H. B.; Scuseria, G. E.; Robb, M. A.; Cheeseman, J. R.; Zakrzewski, V. G.; Montgomery, J. A.; Stratmann, R. E.; Burant, J. C.; Dapprich, S.; Millam, J. M.; Daniels, A. D.; Kudin, K. N.; Strain, M. C.; Farkas, O.; Tomasi, J.; Barone, V.; Cossi, M.; Cammi, R.; Mennucci, B.; Pomelli, C.; Adamo, C.; Clifford, S.; Ochterski, J.; Petersson, G. A.; Ayala, P. Y.; Cui, Q.; Morokuma, K.; Malick, D. K.; Rabuck, A. D.; Raghavachari, K.; Foresman, J. B.; Cioslowki, J.; Ortiz, J. V.; Stefanov, B. B.; Liu, G.; Liashenko, A.; Piskorz, P.; Komaromi, I.; Gomperts, R.; Martin, R. L.; Fox, D. J.; Keith, T.; Al-Laham, M. A.; Peng, C. Y.; Nanayakkara, A.; Gonzalez, C.; Challacombe, M.; Gill, P. M. W.; Johnson, B. G.; Chen, W.; Wong, M. W.; Andres, J. L.; Head-Gordon, M.; Replogle, E. S.; Pople, J. A. *GAUSSIAN 98*; Gaussian, Inc.: Pittsburgh, PA, **1998**.

(40) Beck, A. D. *Phys. Rev. A* **1988**, *38*, 3098.

(41) Perdew, J. P. *Phys. Rev. B* **1986**, *33*, 8822.

(42) Jonas, V.; Frenking, G.; Reetz, M. T. *J. Am. Chem. Soc.* **1994**, *116*, 8741.

(43) Schmidt, A.; Anderson, M. L.; Armstrong, N. R. *J. Appl. Phys.* **1994**, *78*, 5619.
(44) Hopkins, T. A.; Meerholz, K.; Shaheen, S.; Anderson, M. L.; Schmidt, A.; Kippelen, B.; Padias, A. B.; Halls, H. K.; Peyghambarian, N.; Armstrong, N. R. *Chem. Mater.* **1996**, *8*, 344.
(45) Brinkmann, M.; Gadret, G.; Muccini, M.; Taliani, C.; Masciocchi, N.; Sironi, A. *J. Am. Chem. Soc.* **2000**, *122*, 5147.
(46) Burrows, P. E.; Sapochak, L. S.; McCarty, D. M.; Forrest, S. R.; Thompson, M. E. *Appl. Phys. Lett.* **1994**, *64*, 2718.
(47) Humbs, W.; van Veldhoven, E.; Zhang, H.; Glasbeek, M. *Chem. Phys. Lett.* **1999**, *304*, 10.
(48) Garbuzov, D. Z.; Bulovic, V.; Burrows, P. E.; Forrest, S. R. *Chem. Phys. Lett.* **1996**, *249*, 533.
(49) Perkampus, H. H.; Kortüm, K. *Z. Anal. Chem.* **1962**, *190*, 111.